

# On the impact of dark annealing and room temperature illumination on p-type multicrystalline silicon wafers



Carlos Vargas<sup>a,\*</sup>, Gianluca Coletti<sup>a,b</sup>, Catherine Chan<sup>a</sup>, David Payne<sup>a</sup>, Ziv Hameiri<sup>a</sup>

<sup>a</sup> School of Photovoltaic and Renewable Energy Engineering, University of New South Wales, Sydney, Australia

<sup>b</sup> ECN part of TNO – Solar Energy, Petten, the Netherlands

## ARTICLE INFO

### Keywords:

Carrier-induced degradation (CID)  
LeTID  
Multicrystalline silicon (mc-Si)  
Dark anneal  
TIDLS

## ABSTRACT

In the past few years, carrier-induced degradation (CID) in p-type multicrystalline silicon (mc-Si) has been receiving significant attention. Recently, it has been reported that this material is also susceptible to degradation under dark anneal at moderate temperatures. In the first part of this study, we investigate the impact of the dark anneal temperature on mc-Si wafers. We identify both degradation and regeneration of the effective lifetime, where higher temperatures lead to faster rates and lower degradation extent. A fitting model is developed to describe the kinetics of these processes, where the degradation and regeneration process are assumed to happen simultaneously. An Arrhenius analysis of the degradation and regeneration rates, extracted from the proposed model, determines activation energies of  $1.08 \pm 0.05$  eV for the degradation process and  $1.11 \pm 0.04$  eV for the regeneration one. An improvement of the minority carrier effective lifetime of up to 40% is observed after a long dark anneal process. This improvement is associated with enhancement of both the bulk and surface passivation. Temperature- and injection-dependent lifetime spectroscopy measurements indicate that the recombination parameters of the associated defect causing the degradation in the dark are similar to those determined for the CID-related defect; therefore, it seems both defects have a similar nature.

In the second part of the study, the effect of the illumination intensity at room temperature on the degradation/regeneration is studied. Surprisingly, an improvement in the effective lifetime is found, followed by a very slow degradation. The proposed model is found to be suitable to fit these measurements. The extracted rates suggest that the observed behavior is due to a regeneration that is much faster than the degradation.

The reported findings provide new insights into CID in p-type mc-Si that will help improve understanding and assist in developing mitigation solutions.

## 1. Introduction

Degradation of multicrystalline silicon (mc-Si) solar cells under illumination and elevated temperatures was first reported by Ramspeck et al. [1]. Similar degradation was later observed by Kersten et al. [2] who named it light- and elevated temperature-induced degradation (LeTID). Differences in degradation kinetics between open- and short-circuit conditions [2] led some research groups to refer it as carrier-induced degradation (CID) [3,4]; this is the term that will be used in this study. CID/LeTID is currently receiving large attention, as it can lead to efficiency losses of up to 16% (relative) of the passivated emitter and rear cell (PERC) fabricated on mc-Si substrates [5].

It is widely accepted that CID is caused by a bulk-related defect (or defects). Nakayashiki et al. [6] measured a significant reduction of the bulk minority carrier lifetime after light soaking at elevated

temperature. Vargas et al. [7] reported no degradation of the surface passivation quality when monitoring it during CID. Additional evidence of a bulk defect was presented by Padmanabhan et al. [8] as degradation and regeneration were observed on PERC and aluminum back surface field (Al-BSF) cells. Despite the increased research interest in the last years, the bulk defect responsible for CID has not been yet identified. Ramspeck et al. [1] discarded boron-oxygen (B-O) complex as the cause for the degradation, as CID was detected also in gallium (Ga) doped wafers. It is also known that the concentration of interstitial oxygen is considerably lower in mc-Si wafers compare to Czochralski (Cz) wafers [9]. Moreover, the formation rates of CID are much slower than those reported for B-O [1]. They are also slower than the dissociation rate of the iron-boron (Fe-B) pairs. Inglese et al. suggested a possible involvement of copper (Cu) [10]. However, it seems this involvement is not supported by a recent study of Schmid et al. [11], who

\* Corresponding author.

E-mail address: [c.vargascastrillon@student.unsw.edu.au](mailto:c.vargascastrillon@student.unsw.edu.au) (C. Vargas).

measured CID rates of mc-Si wafers contaminated with Cu and other metal impurities.

It is known that CID has a strong dependence on the firing conditions [7,12,13]. CID is less severe in samples fired at low peak temperature (< 600 °C) and it is not present in non-fired samples [12]. In addition, Zuschlag et al. [14] reported different CID behaviors after diffusion and gettering steps, while Chan et al. [15] reported modulation of the CID behavior using an initial dark anneal (DA). In general, it appears that CID has a strong dependence on the thermal history of the mc-Si wafers and cells. Due to the fact that hydrogenated surface passivation layers and the firing step are required for the formation of CID, hydrogen has been suggested as a potential candidate [15–17]. Our recent study using dielectrics containing different hydrogen concentrations provided the first ever experimental support for this suggestion [7]. Involvement of hydrogen in the regeneration was also proposed by Bredemeier et al. [18]; based on their model for CID whereby the regeneration is attributed to the diffusion of the CID defect to the wafer surface, they investigated the CID dependence on wafer thickness and found that the apparent diffusion coefficient of the CID defect was similar to that of hydrogen [18].

Lifetime spectroscopy techniques have been applied to identify the CID-related defect [6,13,19,20]. Based on injection dependent lifetime spectroscopy (IDLS), Nakayashiki et al. [6] determined a capture cross-section ratio [ $k = \sigma_n/\sigma_h$ ; where  $\sigma_{n(h)}$  is the electron (hole) capture cross section] value of 28.5 based on lifetime measurements at room temperature (RT) and assuming a mid-gap defect. Bredemeier et al. [13] also used IDLS at RT to determine  $k = 20 \pm 7$  (assuming a mid-gap defect). Morishige and Jensen et al. [19] reported a defect energy level within the wide range  $-0.27 \text{ eV} < E_t - E_i < 0.13 \text{ eV}$  and  $26 < k < 36$  using a sensitivity analysis of the defect parameters surface solution (DPSS, [21]) curves for IDLS measurements at RT. Tungsten (W), titanium (Ti) and molybdenum (Mo) were suggested as possible candidates. Recently, Vargas and Zhu et al. [20] used temperature- and injection-dependent lifetime spectroscopy (TIDLS) to determine a narrower range of  $E_t - E_i = (-0.32 \pm 0.05) \text{ eV}$  with  $k$  of  $(56 \pm 23)$  or  $E_t - E_i = (0.21 \pm 0.05) \text{ eV}$  with  $k = (49 \pm 21)$ . Unfortunately, the reported uncertainty associated with the recombination parameters of metal impurities is quite wide and therefore several defects can still be considered as candidates. Of course, there is the possibility of a new defect that has not been studied previously.

Recently, Chan et al. [15] reported degradation of mc-Si cells due to DA at moderate temperatures. This work was later extended by Fung et al. [22] confirming degradation due to DA and by Chen et al. [17] who reported similar degradation and lifetime recovery due to DA of B-doped Cz and mc-Si wafers. These studies are the first to show CID without optical or electrical carrier injection. Fung et al. [22] proposed that during DA defect precursors move into the Si bulk from a reservoir. The subsequent DA and light soaking deplete that reservoir and leads to a lower CID extent after a few degradation-regeneration cycles [22]. Based on IDLS analysis, Chen et al. [17] found similar recombination parameters for the CID and DA associated defect in mc-Si; in addition, they found a similar firing dependence of the degradation under illuminated and DA [17]; therefore, they concluded that both defects are likely to have the same nature.

A few approaches have been used in order to determine the time evolution of CID [4,23]. Kwapis et al. [4] found that the degradation rate is proportional to the excess minority carrier concentration ( $\Delta n$ ), suggesting that electrons are associated with the degradation. They used a single exponential function to extract the rates. However, they also suggested an improved fit using two exponential functions to describe slow and fast forming defects, although they also mentioned that the degradation and regeneration can happen simultaneously [4]. Bredemeier et al. [23] used illumination along with thermal treatment (75–120 °C) to degrade the samples. They considered only the degradation part of the kinetics curve to determine the presence of two

defects (fast and slow). Using an Arrhenius analysis they extracted the activation energies of both ( $E_{\text{fast}} = 0.89 \pm 0.04 \text{ eV}$  and  $E_{\text{slow}} = 0.93 \pm 0.06 \text{ eV}$  [23]).

In this contribution, we investigate the temperature dependence, as well as the time evolution, of the degradation and regeneration of p-type mc-Si wafers under DA. We suggest that the degradation and regeneration are happening simultaneously, and propose a model to support this suggestion. TIDLS measurements are used in this work to estimate the recombination parameters of the involved defects. It was confirmed that the DA-related defect is identical to the CID-related defect. Finally, we investigate the dependency of CID on the light intensity at RT.

## 2. Sample preparation and measurement procedure

Ten six-inch neighboring high-performance boron-doped mc-Si wafers from a central brick with a thickness of  $0.0192 \pm 0.0003 \text{ cm}$  and resistivity  $1.70 \pm 0.02 \Omega \text{ cm}$  [bulk doping  $N_A = (8.6 \pm 0.1) \times 10^{15} \text{ cm}^{-3}$ ] were used in this study. Symmetrical lifetime structures were prepared using the front PERC scheme [diffused layer passivated with silicon nitride ( $\text{SiN}_x$ )]: RCA (Radio Corporation of America) cleaning,  $60 \pm 3 \Omega/\square$  phosphorous diffusion (both sides; carried out in a Tempress  $\text{POCl}_3$  tube), hydrofluoric (HF) dip to remove the phosphosilicate glass, a second RCA clean before  $\text{SiN}_x$  deposition onto both sides using a Meyer Burger MAiA plasma enhanced chemical vapour deposition (PECVD) system. The obtained 75 nm  $\text{SiN}_x$  layer (refractive index 2.08 at 630 nm) [24] was then fired in a belt furnace at a sample peak temperature of 800 °C.

The six-inch wafers were then laser cleaved into tokens of  $3.9 \text{ cm} \times 3.9 \text{ cm}$ . The tokens were then split into three groups of sister tokens. **Group I** was dark-annealed using a hotplate (IKA c-mag HS 10) at eight wafer temperatures (138 °C, 160 °C, 176 °C, 203 °C, 228 °C, 254 °C, 275 °C and 300 °C), as measured by a  $k$ -type thermocouple in direct contact with a similar token. **Group II** was used for TIDLS measurements. The wafers were measured before the process and at the most degraded stage, based on the results of Group I. We measured wafers dark annealed at 138 °C, 160 °C, and 176 °C. Wafers of **Group III** were illuminated at RT (20–25 °C) at six light intensities [ $3 \text{ kW/m}^2$  (halogen lamps),  $5 \text{ kW/m}^2$ ,  $10 \text{ kW/m}^2$ ,  $15 \text{ kW/m}^2$ ,  $30 \text{ kW/m}^2$  and  $45 \text{ kW/m}^2$  (all using a 938 nm laser – see below)]. In order to keep the wafers at RT during the illumination, a cooled stage was used (5310 Arroyo Instruments). The sample's temperature under illumination was measured in situ using an infrared thermometer (PC301HT-0, Calex). One token from each group was used as a baseline undergoing the laser-accelerated degradation of Payne et al. [3]. This process was done at temperature of 140 °C using a  $45 \text{ kW/m}^2$  laser.

As Fe was detected in the samples, they were kept in the dark for at least six hours, much longer than the expected association time of Fe-B pairs in this substrate (0.8 h) [25]. The effective lifetime measurements were then taken using a photoconductance (PC) based lifetime tester (WCT-120 from Sinton instruments, actual sample temperature of 30 °C) using the generalized analysis method [26]. These measurements were followed by photoluminescence (PL) images (LIS-R1 from BT Imaging) using an 810 nm laser with a photon flux of  $2.55 \times 10^{17} \text{ cm}^{-2} \text{ s}^{-1}$  and an exposure time of 0.3 s.

The TIDLS measurements were made with a customized lifetime tester at UNSW, whose capabilities include PC and PL measurements, and a wide range of measurement temperatures (-190 to 400 °C) [20]. The measurements were done at sample temperatures of -22 °C, 0, 2 °C, 24 °C, 48 °C and 73 °C, before and after the respective DA treatment (wafers Group II). The Shockley-Read-Hall (SRH) lifetime [27,28] of the defect associated with the DA degradation ( $\tau_{\text{SRH,DA}}$ ) was calculated as the harmonic difference between the non-degraded ( $\tau_{\text{fire}}$ ) and degraded ( $\tau_{\text{deg}}$ ) states effective lifetimes:

$$\tau_{SRH,DA} = \left( \frac{1}{\tau_{deg}} - \frac{1}{\tau_{fire}} \right)^{-1}. \quad (1)$$

$\tau_{SRH,DA}$  was then linearized following the method proposed by Murphy et al. [29]. From the fit of the linearized  $\tau_{SRH,DA}$  to one or two defects, all possible solutions of the defect energy level ( $E_d$ ) and the asymmetry factor ( $k$ ) were plotted following the defect parameter surface solution (DPSS) method [21] and the Newton-Raphson method of Zhu et al. [30]. The defect parameters were obtained from the interceptions of the different DPSS curves.

### 3. Degradation and regeneration kinetics fitting method

We define the normalized effective lifetime as  $\tau_{norm} = \tau(t) / \tau_{fire}$ , where  $\tau(t)$  and  $\tau_{fire}$  are the effective lifetimes at  $\Delta n = 10^{15} \text{ cm}^{-3}$  after a treatment time of  $t$  sec and immediately after firing, respectively. The normalized defect density (NDD) is defined as:

$$\text{NDD}(t) = \left( \frac{1}{\tau(t)} - \frac{1}{\tau_{fire}} \right). \quad (2)$$

Note that NDD is defined here as an amount relative to the state of the sample after firing. The NDD time evolution was fitted using the following expression:

$$\text{NDD}(t) = \text{NDD}_{max} \{ [1 - \exp(-r_{deg} t)] - (1+A)[1 - \exp(-r_{reg} t)] \}, \quad (3)$$

where  $\text{NDD}_{max}$  is the maximum possible NDD,  $A$  is a factor to account for improvement in the effective lifetime (compared to the initial state) due to the process,  $r_{deg}$  and  $r_{reg}$  are the degradation and regenerations rates, respectively. The main differences between this model and the one proposed by Bredemeier et al. [23] are: (i) instead of considering two defects (slow and fast), this model assumes one, (ii) this model assumes degradation and regeneration occur simultaneously, (iii) the maximum amount of defects is related with only one parameter ( $\text{NDD}_{max}$ ) instead of two parameters ( $a$  and  $b$ ) and (iv) the additional factor  $A$  is used to describe the lifetime improvement obtained by the process. One defect is assumed as the linearized lifetime measurements [29] can be fitted very well with one linear fit. This assumption is also supported by previous lifetime spectroscopy measurements that have identified only one defect [19,20,23]. In addition, since the process conditions do not change during the entire time duration, we consider the regeneration to occur simultaneously with the degradation. Note that the model is proposed to describe the kinetics of the degradation and regeneration, independently of the process (light soaking at elevated temperatures or DA). It is a simple semi-empirical approach with good

agreement with our experimental data and it is limited to cases where the rates can be considered constant.

## 4. Results and discussion

### 4.1. Temperature dependence of the degradation under DA

Fig. 1(a) presents the normalized effective lifetime of the tokens dark annealed at eight temperatures in the range of 138–300 °C (Group I). It is compared with the laser-accelerated degradation at 140 °C and light intensity of 45 kW/m<sup>2</sup> (Fig. 1(b)). As the tokens are neighbors and were processed identically, they all have a similar initial effective lifetime (after firing) of  $75 \pm 2 \mu\text{s}$  (at  $\Delta n = 10^{15} \text{ cm}^{-3}$ ).

Higher temperatures lead to both faster degradation and regeneration rates. Note that the wafer processed at 300 °C presents only improvement of the lifetime. The extent of the degradation decreases when the temperature increases. The effective lifetime significantly improves by the process, for some of the wafers improvement in the range of 40% was demonstrated. It is interesting to notice the differences between DA and the baseline laser process (Fig. 1(b)). Although the degradation extent is similar to DA at 160 °C, the rates are much faster. Even more intriguing is the fact that at the end of the laser treatment only a ~7% improvement of the effective lifetime is observed, much smaller than the > 20% of the 160 °C DA case (and > 40% for the DA at higher temperatures). However, this improvement after DA is not stable under light soaking at elevated temperatures [22]; therefore, the involved mechanism associated with the regeneration could be different for both cases. It is also possible that a portion of the observed lifetime improvement is associated with the recovery of pre-existing CID-related defects formed during the firing treatment as suggested by Chen et al. [17]. We assume that this can account for the up to 7% (that is also observed at the end of the laser accelerated process); however, the hydrogen passivation of defects that occurs during firing [31] has much larger impact on the lifetime and prevents us from determining the amount of defects formed during the process. The additional 33% improvement is likely to be related to gettering effects of Fe or other metallic impurities by the phosphorous diffused layer [32], and to other form of hydrogen passivation (surface, crystallographic or other bulk defects) [17,31], as will be discussed in Section 4.3.

Fig. 2 presents the PL images of the sample under DA at 160 °C in different states: Before DA, at the most degraded state and at the end of the DA process, longer treatment times do not induce significant changes in the effective lifetime, indicating saturation. The ratio images are with respect to the image before DA. The images were processed

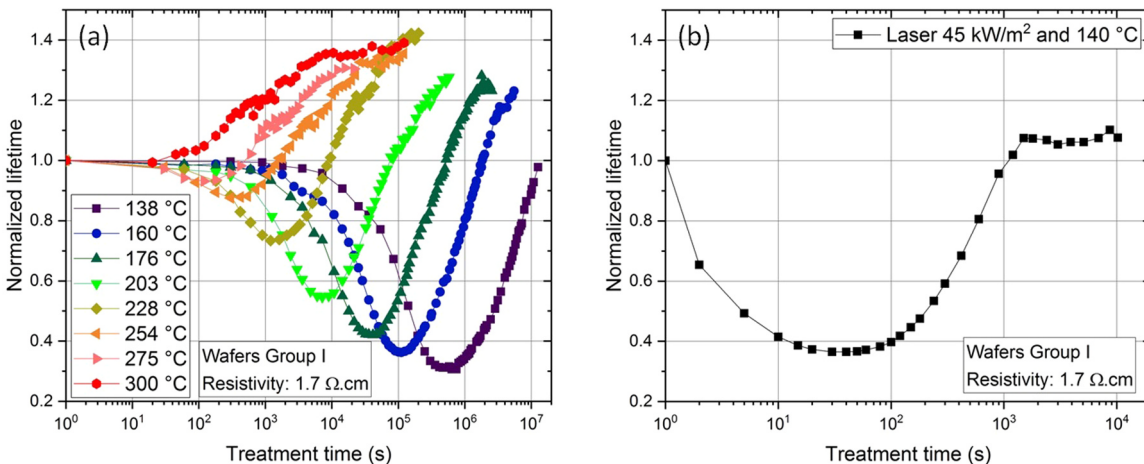
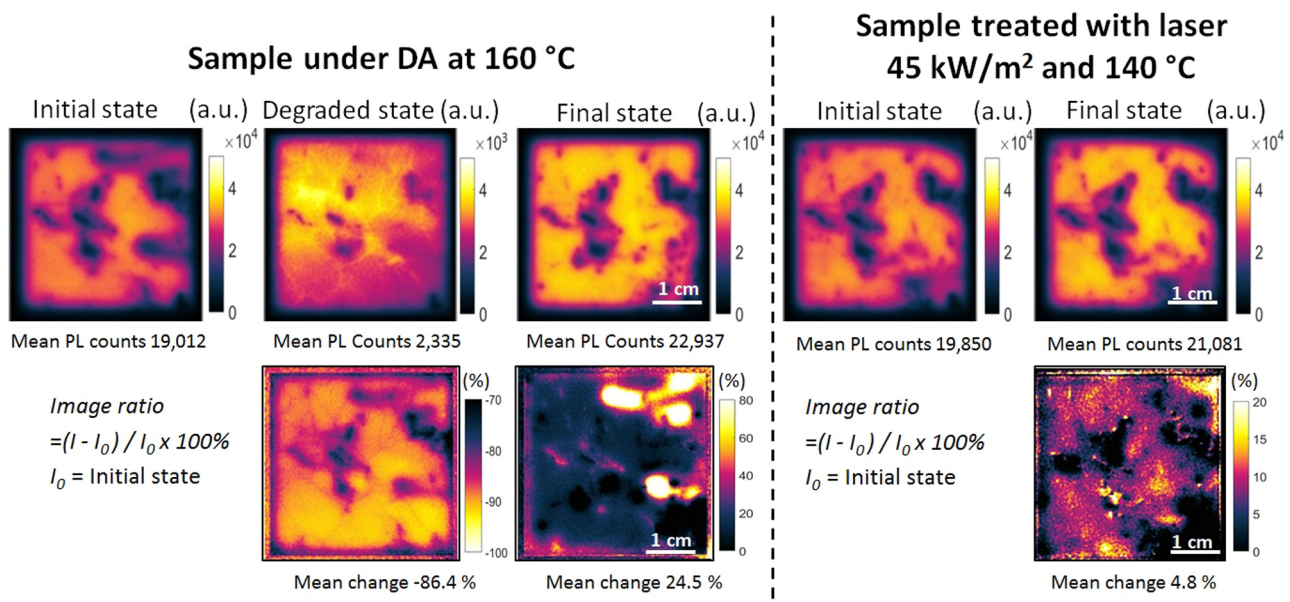


Fig. 1. (a) Evolution of the normalized effective lifetime of wafers dark annealed at different temperatures and (b) evolution of the degradation at 140 °C and 45 kW/m<sup>2</sup>. Note the different time scale. The lines are an aid for the reader.



**Fig. 2.** PL images of the 160 °C DA sample and the baseline of Group I along with the image ratio in the most representative states (please note that different color scales were used for these ratio images to enhance the image contrast).

using a software package described elsewhere [33]. The degradation under DA at 160 °C seems to be quite uniform, with exception of the most dislocated regions and grain boundaries which appear to degrade less. This is in agreement with the observation of Luka et al. under CID conditions [34]. The observed improvement at the end of the process is not uniform as some regions in the wafer appear to improve more than others. Fig. 2 also presents the PL images of the wafer under the laser-accelerated degradation process in the initial and final states. As discussed, much smaller improvement was observed at the end this process, compared to DA at 160 °C.

#### 4.2. Degradation and regeneration rates extraction and activation energies

Fig. 3(a) shows the NDD for the wafers under DA, along with the fits according to the suggested NDD( $t$ ) model (Eq. (3)). These fits have a minimum determination coefficient ( $r^2$ ) of 0.96 (for the 275 °C case), indicating a good agreement between the experimental data and the model. Slight differences were found in the degradation part at low

temperatures ( $T < 200$  °C), while the fit is particularly good for the baseline case ( $r^2 = 0.99$ ), as can be seen in Fig. 3(b). These excellent fits support our suggestion that the process can be described as simultaneous degradation and regeneration processes with different rates, and it is independently of the processes mechanisms, as the model could be used to extract the rates of both DA degradation and CID.

The degradation and regeneration rates are presented using an Arrhenius plot in Fig. 4(a). We consider a 2 °C uncertainty in the measured temperatures (error bars of the x-axis). The error bars of the y-axis represents the uncertainty associated with the fitting, based on the 95% confidence bounds method as implemented in Matlab [35]. The Arrhenius function was defined as

$$r_{deg/reg} = C \times \exp\left(-\frac{E_{deg/reg}}{k_B T}\right) , \quad (4)$$

where  $C$  is a constant,  $k_B$  is the Boltzmann constant,  $T$  is the temperature and  $E_{deg/reg}$  are the degradation and regeneration activation

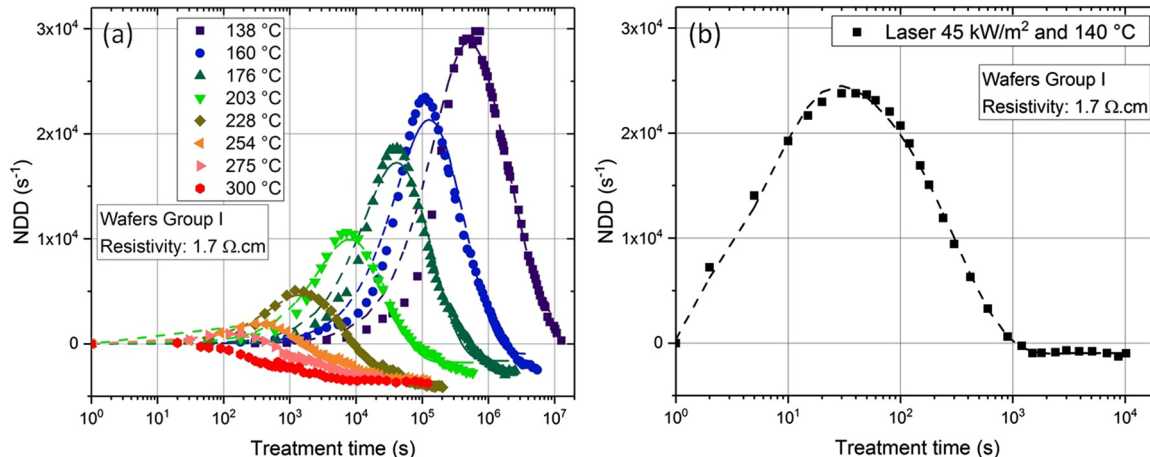


**Fig. 3.** NDD evolution along with the fit using Eq. (3) (dashed lines): (a) Wafers under DA at different temperatures and (b) wafer under laser-accelerated degradation. Note the different time scale.

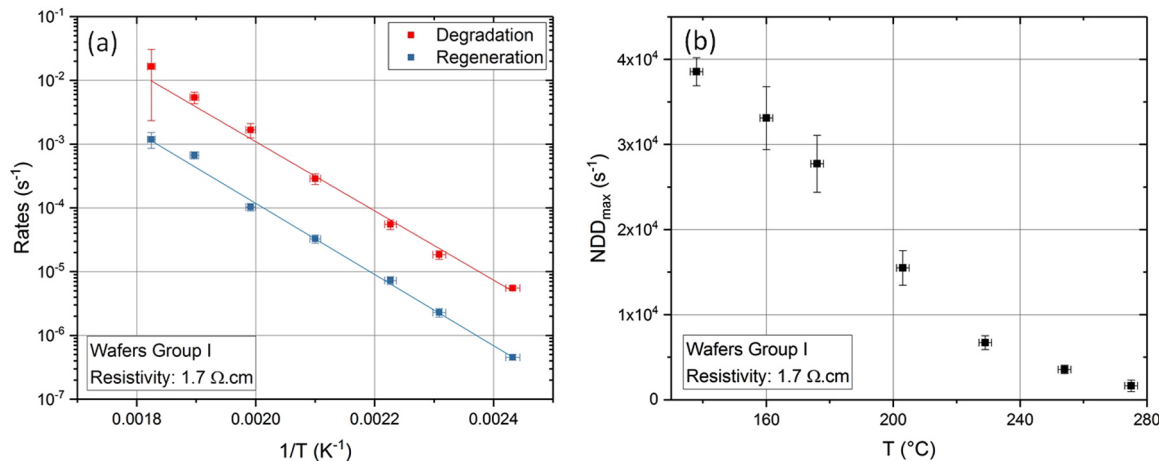


**Fig. 4.** Fit parameters: (a) Degradation and regeneration rates for the different DA temperatures, the lines correspond to a fit to the Arrhenius analysis, and (b)  $\text{NDD}_{\max}$  versus the process temperatures.

energies, respectively. We determined activation energy of  $1.08 \pm 0.05 \text{ eV}$  for the degradation process and  $1.11 \pm 0.04 \text{ eV}$  for the regeneration process. The similarity between the activation energies of the degradation and regeneration processes indicates that both reactions may have a similar cause. This particular fact is compatible with the involvement of hydrogen in the degradation and regeneration processes, as recently suggested [7,15,16].

The obtained values are slightly different from the ones reported by Bredemeier *et al.* for the fast and slow defects ( $E_{\text{fast}} = 0.89 \pm 0.04 \text{ eV}$  and  $E_{\text{slow}} = 0.93 \pm 0.06 \text{ eV}$  [23]). The difference can be explained by the fact that Bredemeier *et al.* [23] extracted the rates with samples under illumination and they only considered the degradation part of the kinetics. It is highly likely that the light accelerates the degradation and regeneration processes, as indicated by comparison of DA at  $138 \text{ °C}$  and the baseline, leading to an underestimation of the activation energies. Additionally, it is possible that the degradation mechanisms are different (DA and CID) due to their stability [22], therefore their activation energies could be different.

Fig. 4(b) presents  $\text{NDD}_{\max}$  as a function of temperature. Again, a strong dependence on the temperature can be observed, with higher temperatures lead to a smaller  $\text{NDD}_{\max}$ .

#### 4.3. Surface saturation current density and high injection bulk lifetime changes

Changes in the surface passivation quality are often overlooked, as most studies have focused on changes in the *effective* lifetime. In order to consider variations of the surface passivation during the processes (both DA and laser-based), the high injection *bulk* lifetime ( $\tau_{\text{Bulk}}$ ) and the surface saturation current density ( $J_{0s}$ ) were extracted at  $\Delta n = 1.5 \times 10^{16} \text{ cm}^{-3}$  based on the Kane and Swanson method [36] as implemented in the Sinton lifetime tester. The obtained trends were confirmed by modelling using Quokka version 2 [37]. The normalized extracted values are presented in Fig. 5 (note that similar values were extracted for all the wafers:  $\tau_{\text{Bulk}} = 154 \pm 5 \mu\text{s}$  and  $J_{0s} = 95 \pm 2 \text{ fA cm}^{-2}$  after firing). The normalized  $\tau_{\text{Bulk}}$  graphs (Fig. 5(a) and Fig. 5(b)) demonstrate a similar trend to the ones observed for the effective lifetime (Fig. 1); the differences between them can be explained by the changes in  $J_{0s}$  (Fig. 5(c) and (d)) and the injection dependence of the SRH recombination. It seems that the surface passivation quality improved during both DA and the laser processes (Fig. 5(c) and (d)). This improvement is faster at higher temperatures. A deeper investigation regarding the changes in the surface passivation quality during DA is presented in Ref. [38] and illuminated anneal Refs.

[39,40]. To investigate the impact of the changes in the surface passivation during the process, we re-analyze the NDD considering  $\tau_{\text{Bulk}}$  at high injection (Eq. (2)). The fits have a similar quality to that of Fig. 3, with the exception of the measurement at  $275 \text{ °C}$ , which has a large uncertainty in the fit. Using an Arrhenius-based analysis (Eq. (4)), the activation energies were determined to be very similar the ones obtained using the effective lifetime:  $1.04 \pm 0.06 \text{ eV}$  for the degradation process and  $1.05 \pm 0.04 \text{ eV}$  for the regeneration process.

#### 4.4. Recombination parameters of the DA-related defect

TIDLS measurements were done for the dark annealed wafers of Group II. For this analysis, we selected wafers that showed high degradation extents (DA at  $138 \text{ °C}$ ,  $160 \text{ °C}$  and  $176 \text{ °C}$ ). A smaller extent of the degradation can lead to a larger uncertainty in the extracted SRH defect lifetime. Representative DPSS curves of the  $138 \text{ °C}$  wafer are presented in Fig. 6(a), while the DPSS curves of the baseline (laser treated) wafer are presented in Fig. 6(b) for a comparison.

The extracted SRH parameters are summarized in Table 1. The uncertainty ranges associated with the energy level ( $E_t - E_i$ , where  $E_i$  is the intrinsic energy level of silicon) and the asymmetry factor ( $k$ ) of the DA-related defect includes the three measured samples ( $138 \text{ °C}$ ,  $160 \text{ °C}$  and  $176 \text{ °C}$ ). The values extracted of the DA-related defect are within the range of the accelerated degradation (baseline) and of the ones we determined for the CID-related defect in our previous study [20], pointing that both degradations (DA and CID) are caused by the same defect. This is in agreement with Chen *et al.*, who reported that both degradations have the same  $k$ , assuming the energy level of both defects in the mid-gap [17].

Although both defects appear to be the same, the recovery mechanisms under dark and illuminated annealing appear to be different due to the resulting stability differences as discussed previously. To date, these mechanisms remain unknown. A similar behavior has been observed for the well-known B-O complex, where the stability of the recovered lifetime has been found to dependent on whether annealing is performed in the dark or with illumination [41]. The non-permanent recovery of the lifetime during dark annealing is often thought to be just a reversal of the defect formation process, transitioning the defect into its precursor species via a dissociation reaction [42], whilst the permanent recovery in lifetime during illuminated annealing has been attributed to hydrogen passivation of the B-O defect [43]. Further investigation is required to establish the respective recovery mechanisms of CID due to dark or illuminated anneals.

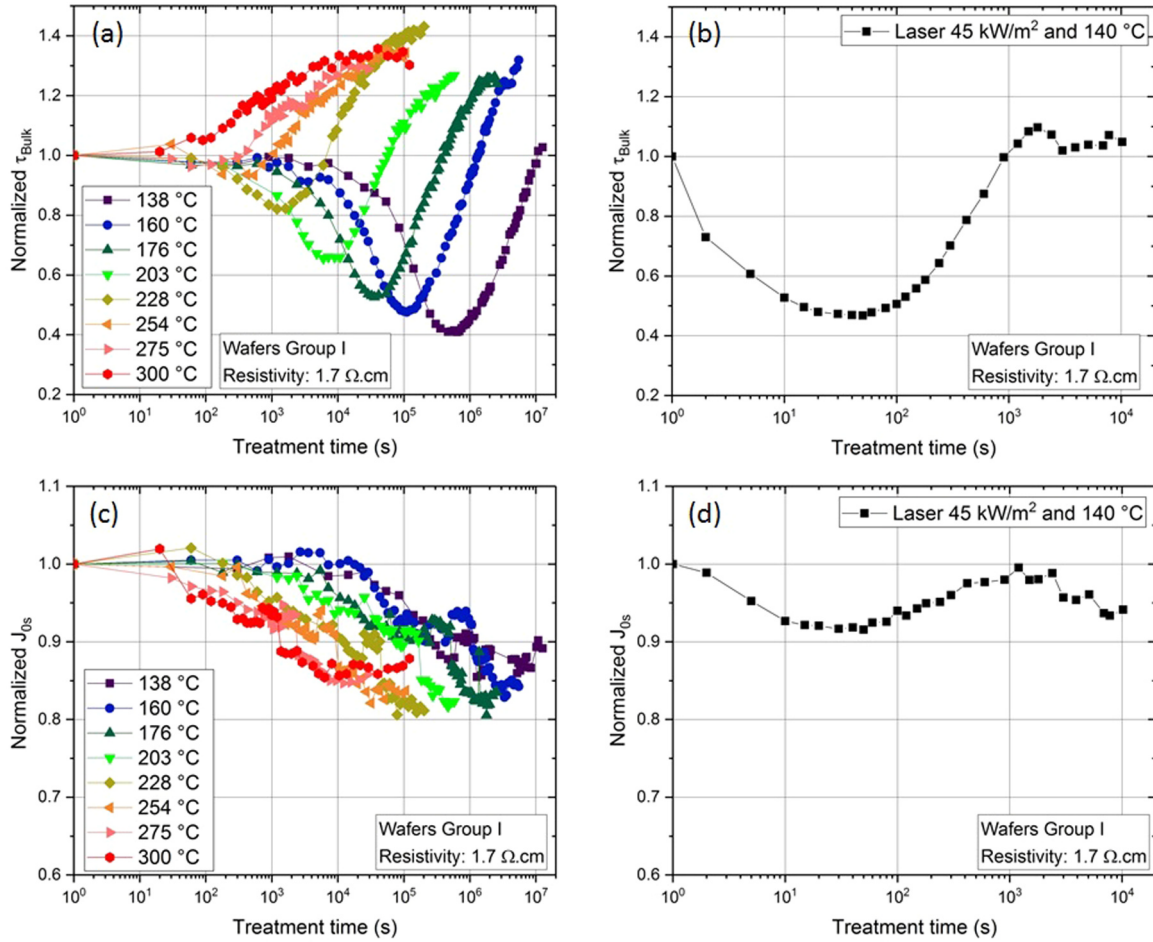


**Fig. 5.** Extracted normalized high injection bulk lifetime of Group I under (a) DA, and (b) accelerated laser degradation. The surface saturation current density of the same group under (c) DA, and (d) accelerated laser degradation. The lines are an aid for the reader. Note the different time scale.

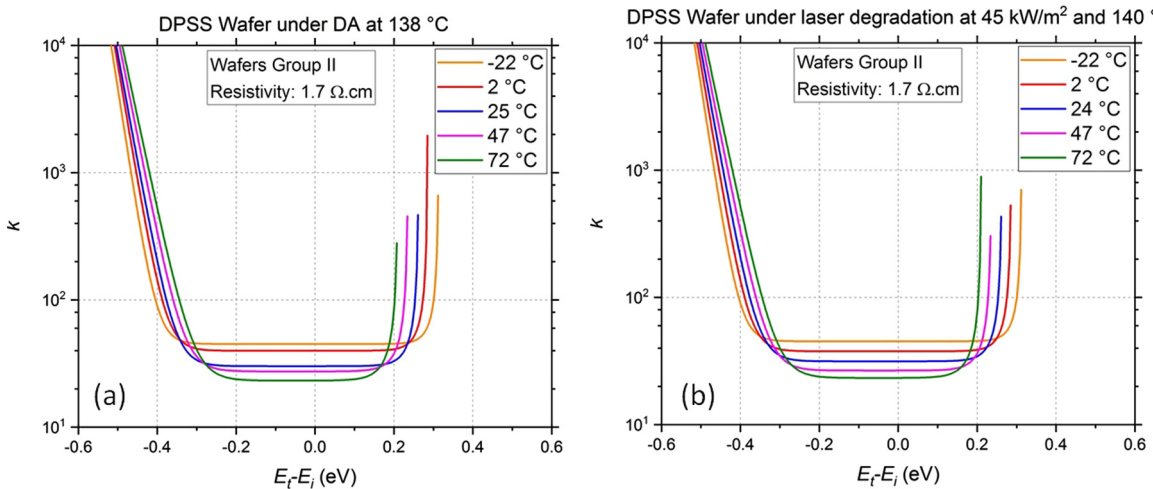


**Fig. 6.** (a) DPSS for the dominant defect of a sample degraded using DA at 138 °C, (b) DPSS of the CID-related defect using a similar token treated with the laser at 140 °C and 45 kW/m<sup>2</sup>.

**Table 1**  
Recombination parameters of the defects measured by TIDLS.

| Band-gap half | Parameter        | DA-related defect | CID (Fig. 7(b))  | CID (Vargas and Zhu et al. [20]) |
|---------------|------------------|-------------------|------------------|----------------------------------|
| Bottom        | $E_t - E_i$ (eV) | $-0.31 \pm 0.05$  | $-0.31 \pm 0.05$ | $-0.32 \pm 0.05$                 |
|               | $k$              | $46 \pm 16$       | $40 \pm 11$      | $56 \pm 23$                      |
| Upper         | $E_t - E_i$ (eV) | $0.21 \pm 0.05$   | $0.20 \pm 0.05$  | $0.22 \pm 0.05$                  |
|               | $k$              | $45 \pm 15$       | $38 \pm 10$      | $49 \pm 21$                      |

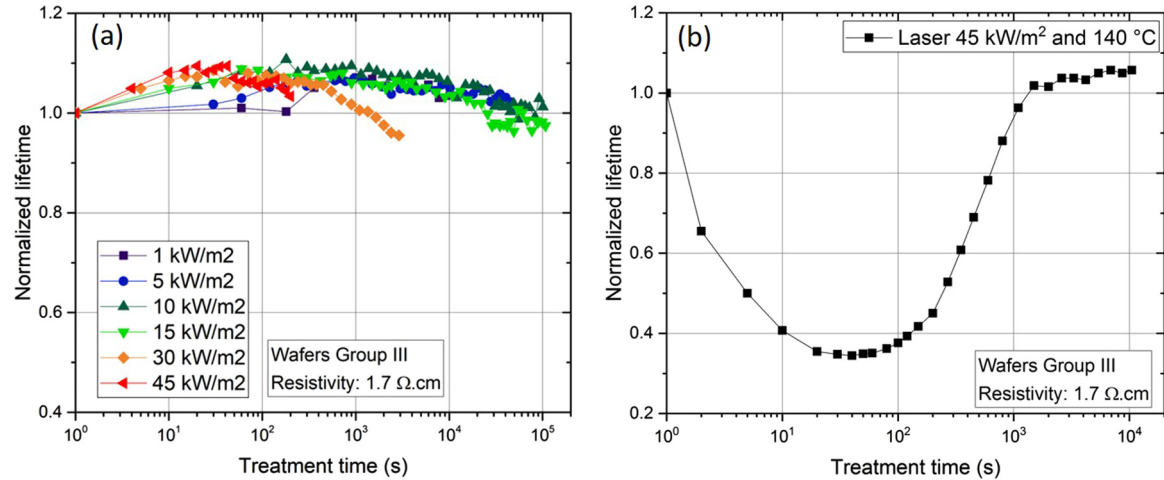


**Fig. 7.** (a) Evolution of the normalized effective lifetime of the tokens from Group III under different light intensities at RT. (b) The lifetime evolution of a token from the same group under accelerated laser degradation. Note the different time scale. The lines are an aid for the reader.

#### 4.5. Effect of high intensity illumination at RT

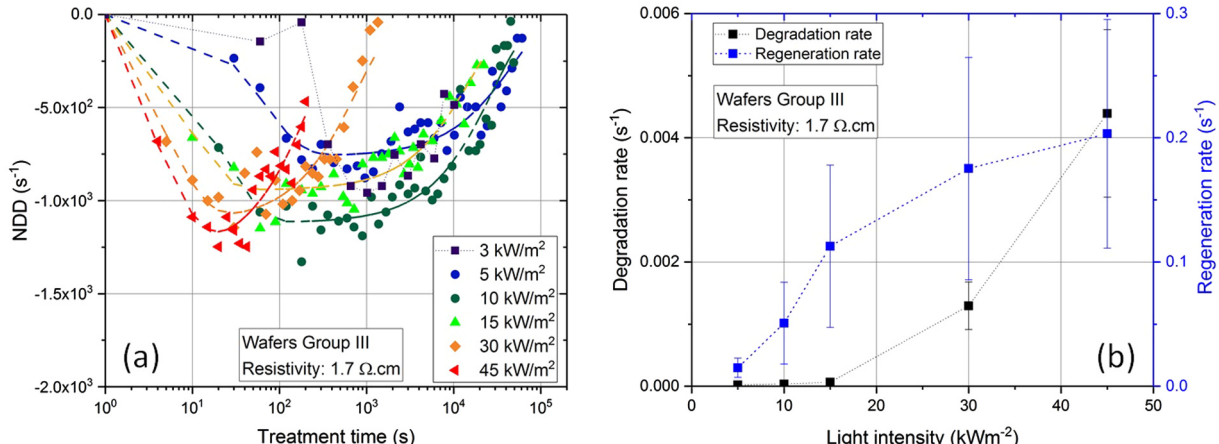
We now investigate samples that were treated with different illumination intensities at temperatures around RT. To our knowledge, this is the first investigation of the effect of illumination on *p*-type mc-Si at temperatures around RT. Fig. 7(a) presents the evolution of the effective lifetime at six light intensities, the initial value (after firing) of the tokens from this group was  $71 \pm 2 \mu\text{s}$  (at  $\Delta n = 10^{15} \text{ cm}^{-3}$ ). Surprisingly, an initial lifetime improvement of around 10% was observed for all the light intensities, it is then followed by a very slow degradation. Wafers that were treated at high light intensities improved and degraded faster. The dissociation of the Fe-B pairs was discarded as a possible explanation of the observed change, as the effective lifetimes were measured at least six hours after each illumination process.

Fig. 8(a) presents the calculated NDD for this process based on Eq. (2). In this study, we define negative NDD values as an improvement of the effective lifetime compared to the initial state. The model developed above for DA (see Eq. (3)) was then used to fit these NDD curves, they are also included in the figure. A minimum  $r^2$  of 0.78 (for the sample under 5 kW/m<sup>2</sup>), indicating an acceptable fit quality. The observed improvement of the effective lifetime can be explained by the fact that the regeneration is much faster than the degradation. This regeneration is more likely to be related with defects formed after the firing [17], as indicated by the final lifetime of the baseline of Group III (Fig. 7(b)), which is ~6% higher than the initial value. At this stage, the

information associated with the degradation part is limited and imposes a large uncertainty on the estimated degradation rates (see Fig. 8(b)) and therefore was omitted. It seems that the degradation and regeneration rates increase with the light intensity. However, due to the significant uncertainty associated with the obtained values, several other dependencies of the rates on the light intensity are possible. These results are in agreement with the linear dependence of the CID degradation rate with  $\Delta n$ , reported by Kwaplil *et al.* [4] using electrical carrier injection at 75 °C.

#### 5. Conclusions

The temperature dependence of *p*-type mc-Si degradation due to annealing in the dark has been studied. Differences in the rates and degradation extents were determined. It was shown that high temperature leads to faster degradation and regeneration, and lower degradation extent. A new model to extract the degradation and regeneration rates has been proposed, with a good agreement with the experimental data and where all the constants have appropriated physical meaning. We explain the degradation-regeneration curve using only one defect assuming that the degradation and regeneration are happening simultaneously. Based on the extracted rates, the activation energies for the degradation and regeneration processes were determined to be  $1.08 \pm 0.05 \text{ eV}$  and  $1.11 \pm 0.04 \text{ eV}$ , respectively. An improvement of the minority carrier lifetime up to 40% was observed at



**Fig. 8.** (a) Evolution of the NDD of the tokens under illumination at room temperature, the dashed lines correspond to the fits. (b) Extracted rates as a function of the light intensity. The lines are an aid for the reader.

high temperatures, with the similar trend at low temperatures, which was found to be associated to both a bulk and surface passivation improvements.

Based on TIDLS the recombination parameters of the defect associated with the degradation under DA were measured to be:  $E_t - E_i = -0.31 \pm 0.05$  eV and  $k = 46 \pm 16$  (bottom band-gap half), and  $E_t - E_i = 0.21 \pm 0.05$  eV and  $k = 45 \pm 15$  (upper band-gap half). These are similar to those of the CID-related defect, indicating that they are likely to be caused by the same defect.

The effect of light at room temperature on *p*-type mc-Si wafers was found to be a lifetime improvement, followed by a slow degradation. The extracted rates using the model proposed for the DA indicate that the regeneration is happening faster than the degradation. To our knowledge, this is the first time that such observation is reported. This opens the question of what role light plays in CID.

The reported findings provide additional information regarding the kinetics and properties of the CID-related defect in *p*-type mc-Si. This additional information will help the scientific community to determine

the root cause of this defect and to find solutions to mitigate it.

### Acknowledgments

The authors acknowledge support from the Australian Government through the Australian Renewable Energy Agency (ARENA, Project 2014/RND097). The views expressed herein are not necessarily the views of the Australian Government, and the Australian Government does not accept responsibility for any information or advice contained herein. Z. Hameiri acknowledges the support of the Australian Research Council (ARC) through the Discovery Early Career Researcher Award (DECRA, Project DE150100268). The authors also acknowledge ECN part of TNO – Solar Energy “Advanced hydrogenation and silicon materials” project, the help from the Solar Industrial Research Facility (SIRF) team of UNSW for their help in the sample preparation and Y. Zhu for the program to perform the TIDLS analysis. Special thanks to Professor Stuart Wenham who sadly passed away recently for his many valuable comments, advice and suggestions.

### Appendix A. Stability of a sample with previous dark anneal

See Fig. A1

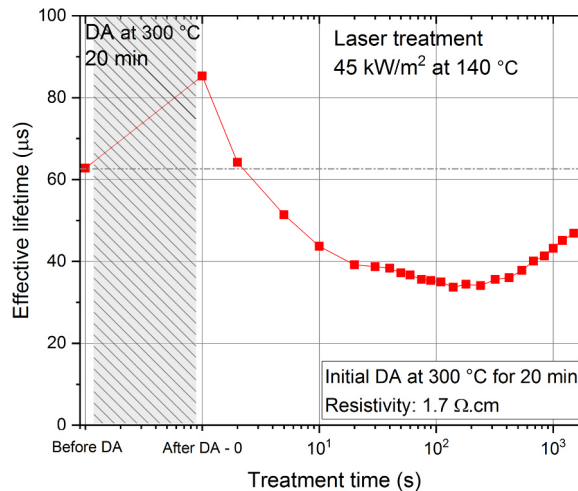


**Fig. A-1.** Evolution of the effective lifetime extracted at  $\Delta n = 1.0 \times 10^{15} \text{ cm}^{-3}$  for a sample that initially received DA at 300 °C for 20 min and then went to the laser accelerated degradation process at 45 kW/m² and 140 °C. Significant degradation can be observed, but with a reduced extent and slower rate than the sample with no pre-DA shown in Fig. 1(b). This is consistent with results presented in [15]. The lines are an aid for the reader.

### References

- [1] K. Ramspack, S. Zimmermann, H. Nagel, A. Metz, Y. Gassenbauer, B. Birkmann, A. Seidl, Light induced degradation of rear passivated mc-Si solar cells, 27th Eur. Photovolt. Sol. Energy Conference Exhib (2012) pp. 861–865. doi:[10.4229/27thEUPVSEC.2012-2DO.3.4](https://doi.org/10.4229/27thEUPVSEC.2012-2DO.3.4).
- [2] F. Kersten, P. Engelhart, H.-C. Ploigt, A. Stekolnikov, T. Lindner, F. Stenzel, M. Bartsch, A. Szpath, K. Petter, J. Heitmann, J.W. Müller, Degradation of multicrystalline silicon solar cells and modules after illumination at elevated temperature, Sol. Energy Mater. Sol. Cells 142 (2015) 83–86, <https://doi.org/10.1016/j.solmat.2015.06.015>.
- [3] D.N.R. Payne, C.E. Chan, B.J. Hallam, B. Hoex, M.D. Abbott, S.R. Wenham, D.M. Bagnall, Acceleration and mitigation of carrier-induced degradation in *p*-type multi-crystalline silicon, Phys. Status Solidi. Res. Lett. 10 (2016) 237–241, <https://doi.org/10.1002/pssr.201510437>.
- [4] W. Kwapisl, T. Niewelt, M.C. Schubert, Kinetics of carrier-induced degradation at elevated temperature in multicrystalline silicon solar cells, Sol. Energy Mater. Sol. Cells 173 (2017) 80–84, <https://doi.org/10.1016/j.solmat.2017.05.066>.
- [5] K. Petter, K. Hübener, F. Kersten, M. Bartsch, F. Fertig, B. Klöter, J. Müller, Dependence of LeTID on brick height for different wafer suppliers with several resistivities and dopants, presented at the 9th Int. Work. Cryst. Silicon Sol. Cells (2016).
- [6] K. Nakayashiki, J. Hofstetter, A.E. Morishige, T.T.A. Li, D.B. Needleman, M.A. Jensen, T. Buonassisi, Engineering solutions and root-cause analysis for light-induced degradation in *p*-type multicrystalline silicon PERC modules, IEEE J. Photovolt. 6 (2016) 860–868, <https://doi.org/10.1109/JPHOTOV.2016.2556981>.
- [7] C. Vargas, K. Kim, G. Coletti, D. Payne, C. Chan, S. Wenham, Z. Hameiri, Carrier-induced degradation in multicrystalline silicon: dependence on the silicon nitride passivation layer and hydrogen released during firing, IEEE J. Photovolt. 8 (2018) 413–420, <https://doi.org/10.1109/JPHOTOV.2017.2783851>.
- [8] M. Padmanabhan, K. Jhaveri, R. Sharma, P.K. Basu, S. Raj, J. Wong, J. Li, Light-induced degradation and regeneration of multicrystalline silicon Al-BSF and PERC solar cells, Phys. Status Solidi - Rapid Res. Lett. 10 (2016) 874–881, <https://doi.org/10.1002/pssr.201600173>.
- [9] G. Coletti, C.L. Mulder, G. Galbiati, L.J. Geerligs, Reduced effect of B-O degradation on multicrystalline silicon wafers, in: Proceedings of the 21st Eur. Photovolt. Sol. Energy Conference Exhib., Dresden, Germany (2006) pp. 1515–1518.
- [10] A. Inglese, A. Focareta, F. Schindler, J. Schön, J. Lindroos, M.C. Schubert, H. Savin, Light-induced degradation in multicrystalline silicon: the role of copper, Energy Procedia 92 (2016) 808–814, <https://doi.org/10.1016/j.egypro.2016.07.073>.
- [11] A. Schmid, A. Zuschlag, D. Skorka, J. Fritz, C. Winter, G. Hahn, Influence of different transition metal contaminations on degradation and regeneration in mc Si, in: Proceedings of the 33rd Eur. Photovolt. Sol. Energy Conference Exhib. (2017) pp. 321–324. doi:[10.4229/EUPVSEC.20172017-2BO.2.2](https://doi.org/10.4229/EUPVSEC.20172017-2BO.2.2).
- [12] C.E. Chan, D.N.R. Payne, B.J. Hallam, M.D. Abbott, T.H. Fung, A.M. Wenham, B.S. Tjahjono, S.R. Wenham, Rapid stabilization of high-performance multicrystalline *p*-type silicon PERC cells, IEEE J. Photovolt. 6 (2016) 1473–1479, <https://doi.org/10.1109/JPHOTOV.2016.2606704>.
- [13] D. Bredemeier, D. Walter, S. Herlufsen, J. Schmidt, Lifetime degradation and regeneration in multicrystalline silicon under illumination at elevated temperature, AIP Adv. 6 (2016) 035119, <https://doi.org/10.1063/1.4944839>.

- [14] A. Zuschlag, D. Skorka, G. Hahn, Degradation and regeneration in mc-Si after different gettering steps, *Prog. Photovolt. Res. Appl.* 25 (2017) 545–552, <https://doi.org/10.1002/pip.2832>.
- [15] C. Chan, T.H. Fung, M. Abbott, D. Payne, A. Wenham, B. Hallam, R. Chen, S. Wenham, Modulation of carrier-induced defect kinetics in multi-crystalline silicon PERC cells through dark annealing, *Phys. Status Solidi. Res. Lett.* 1 (2017) 1600028, <https://doi.org/10.1002/solr.201600028>.
- [16] M.A. Jensen, A.E. Morishige, J. Hofstetter, D.B. Needleman, T. Buonassisi, Evolution of LeTID defects in p-type multicrystalline silicon during degradation and regeneration, *IEEE J. Photovolt.* 7 (2017) 980–987, <https://doi.org/10.1109/JPHOTOV.2017.2695496>.
- [17] D. Chen, M. Kim, B.V. Stefani, B.J. Hallam, M.D. Abbott, C.E. Chan, R. Chen, D.N.R. Payne, N. Nampalli, A. Ciesla, T.H. Fung, K. Kim, S.R. Wenham, Evidence of an identical firing-activated carrier-induced defect in monocrystalline and multicrystalline silicon, *Sol. Energy Mater. Sol. Cells* 172 (2017) 293–300, <https://doi.org/10.1016/j.solmat.2017.08.003>.
- [18] D. Bredemeier, D.C. Walter, J. Schmidt, Possible candidates for impurities in mc-Si wafers responsible for light-induced lifetime degradation and regeneration, *Phys. Status Solidi - Rapid Res. Lett.* 2 (2018) 1700159, <https://doi.org/10.1002/solr.201700159>.
- [19] A.E. Morishige, M.A. Jensen, D.B. Needleman, K. Nakayashiki, J. Hofstetter, T.T.A. Li, T. Buonassisi, Lifetime spectroscopy investigation of light-induced degradation in p-type multicrystalline silicon PERC, *IEEE J. Photovolt.* 6 (2016) 1466–1472, <https://doi.org/10.1109/JPHOTOV.2016.2606699>.
- [20] C. Vargas, Y. Zhu, G. Coletti, C. Chan, D. Payne, M. Jensen, Z. Hameiri, Recombination parameters of lifetime-limiting carrier-induced defects in multicrystalline silicon for solar cells, *Appl. Phys. Lett.* 110 (2017) 092106, <https://doi.org/10.1063/1.4977906>.
- [21] Stefan Rein, *Lifetime spectroscopy a method of defect characterization in silicon for photovoltaics applications*, First, Springer-Verlag, Germany, 2005.
- [22] T.H. Fung, C.E. Chan, B.J. Hallam, D.N.R. Payne, M.D. Abbott, S.R. Wenham, Impact of annealing on the formation and mitigation of carrier-induced defects in multi-crystalline silicon, *Energy Procedia* 124 (2017) 726–733, <https://doi.org/10.1016/j.egypro.2017.09.087>.
- [23] D. Bredemeier, D. Walter, J. Schmidt, Light-induced lifetime degradation in high-performance multicrystalline silicon: detailed kinetics of the defect activation, *Sol. Energy Mater. Sol. Cells* 173 (2017) 2–5, <https://doi.org/10.1016/j.solmat.2017.08.007>.
- [24] Z. Hameiri, N. Borojevic, L. Mai, N. Nandakumar, K. Kim, S. Winderbaum, Low-absorbing and thermally stable industrial silicon nitride films with very low surface recombination, *IEEE J. Photovolt.* 7 (2017) 996–1003, <https://doi.org/10.1109/JPHOTOV.2017.2706424>.
- [25] D. Macdonald, T. Roth, P.N.K. Deenapanray, K. Bothe, P. Pohl, J. Schmidt, Formation rates of iron-acceptor pairs in crystalline silicon, *J. Appl. Phys.* 98 (2005) 083509, <https://doi.org/10.1063/1.2102071>.
- [26] H. Nagel, C. Berge, A.G. Aberle, Generalized analysis of quasi-steady-state and quasi-transient measurements of carrier lifetimes in semiconductors, *J. Appl. Phys.* 86 (1999) 6218–6221, <https://doi.org/10.1063/1.371633>.
- [27] W. Shockley, W.T. Read, Statistics of the recombinations of holes and electrons, *Phys. Rev.* 87 (1952) 835–842, <https://doi.org/10.1103/PhysRev.87.835>.
- [28] R.N. Hall, Electron-hole recombination in germanium, *Phys. Rev.* 87 (1952), <https://doi.org/10.1103/PhysRev.87.387> ((387–387)).
- [29] J.D. Murphy, K. Bothe, R. Krain, V.V. Voronkov, R.J. Falster, Parameterisation of injection-dependent lifetime measurements in semiconductors in terms of Shockley-Read-Hall statistics: an application to oxide precipitates in silicon, *J. Appl. Phys.* 111 (2012) 113709, <https://doi.org/10.1063/1.4725475>.
- [30] Y. Zhu, Q.T.L. Gia, M.K. Juhl, G. Coletti, Z. Hameiri, Application of the Newton-Raphson method to lifetime spectroscopy for extraction of defect parameters, *IEEE J. Photovolt.* 7 (2017) 1092–1097, <https://doi.org/10.1109/JPHOTOV.2017.2695666>.
- [31] L.J. Geerligs, Y. Komatsu, I. Röver, K. Wambach, I. Yamaga, T. Saitoh, Precipitates and hydrogen passivation at crystal defects in n- and p-type multicrystalline silicon, *J. Appl. Phys.* 102 (2007) 093702, <https://doi.org/10.1063/1.2800271>.
- [32] M. Rinio, A. Yodyunyong, S. Keipert-Colberg, Y.P.B. Mouafi, D. Borchert, A. Montesdeoca-Santana, Improvement of multicrystalline silicon solar cells by a low temperature anneal after emitter diffusion, *Prog. Photovolt. Res. Appl.* 19 (2011) 165–169, <https://doi.org/10.1002/pip.1002>.
- [33] D.N.R. Payne, C. Vargas, Z. Hameiri, S.R. Wenham, D.M. Bagnall, An advanced software suite for the processing and analysis of silicon luminescence images, *Comput. Phys. Commun.* 215 (2017) 223–234, <https://doi.org/10.1016/j.cpc.2017.02.012>.
- [34] T. Luka, S. Großer, C. Hagendorf, K. Ramspeck, M. Turek, Intra-grain versus grain boundary degradation due to illumination and annealing behavior of multi-crystalline solar cells, *Sol. Energy Mater. Sol. Cells* 158 (2016) 43–49, <https://doi.org/10.1016/j.solmat.2016.05.061>.
- [35] MathWorks, PDF documentation for curve fitting toolbox. <[https://au.mathworks.com/help/pdf\\_doc/curvefit/index.html](https://au.mathworks.com/help/pdf_doc/curvefit/index.html)> (Accessed 9 April 2018).
- [36] D. Kane, R. Swason, Measurement of the emitter saturation current by a contactless photoconductivity decay method, 18th IEEE Photovolt. Spec. Conference 18 (1985) pp. 578–583.
- [37] A. Fell, K.R. McIntosh, M. Abbott, D. Walter, A. Quokka version 2: selective surface doping, luminescence modeling and data fitting, in: Proceedings of the 23rd Photovolt. Sci. Eng. Conference.
- [38] K. Kyung, R. Chen, D. Chen, S. Wenham, Z. Hameiri, Surface passivation degradation at elevated temperature of monocrystalline silicon wafers, *IEEE J. Photovolt.* Submitted for publication (2018).
- [39] D. Sperber, A. Graf, D. Skorka, A. Herguth, G. Hahn, Degradation of surface passivation on crystalline silicon and its impact on light-induced degradation experiments, *IEEE J. Photovolt.* 7 (2017) 1627–1634, <https://doi.org/10.1109/JPHOTOV.2017.2755072>.
- [40] D. Sperber, A. Heilemann, A. Herguth, G. Hahn, Temperature and light-induced changes in bulk and passivation quality of boron-doped float-zone silicon coated with SiNx:H, *IEEE J. Photovolt.* 7 (2017) 463–470, <https://doi.org/10.1109/JPHOTOV.2017.2649601>.
- [41] A. Herguth, G. Schubert, M. Kaes, G. Hahn, A new approach to prevent the negative impact of the metastable defect in boron doped CZ silicon solar cells, in: Conference Rec IEEE 4th World Conference Photovolt. Energy Convers (2006) : pp. 940–943. doi:[10.1109/WCPEC.2006.279611](https://doi.org/10.1109/WCPEC.2006.279611).
- [42] B. Lim, K. Bothe, J. Schmidt, Deactivation of the boron–oxygen recombination center in silicon by illumination at elevated temperature, *Phys. Status Solidi – Rapid Res. Lett.* 2 (2008) 93–95, <https://doi.org/10.1002/pssr.200802009>.
- [43] B.J. Hallam, S.R. Wenham, P.G. Hamer, M.D. Abbott, A. Sugianto, C.E. Chan, A.M. Wenham, M.G. Eadie, G. Xu, Hydrogen passivation of B-O defects in Czochralski silicon, *Energy Procedia* 38 (2013) 561–570, <https://doi.org/10.1016/j.egypro.2013.07.317>.